The Phase State of Poly(butadiene-*b*-*tert*-butyl methacrylate) and Poly(ethylene-*b*-*tert*-butyl methacrylate) Diblock Copolymers

F. J. M. Schipper,[†] G. Floudas,*[,†,‡] S. Pispas,[§] N. Hadjichristidis,[§] and T. Pakula[⊥]

Foundation for Research and Technology-Hellas, IESL, P.O. Box 1527, 71110 Heraklion, Crete, Greece; Department of Physics, University of Ioannina, P.O. Box 1186, 451 10 Ioannina, Greece and Biomedical Research Institute (BRI-FORTH), Ioannina, Greece; Department of Chemistry, University of Athens, Zografou 15771, Athens, Greece; and Max-Planck Institut für Polymerforschung, Postfach 3148, 55021 Mainz, Germany

Received April 5, 2002

ABSTRACT: We report on the phase state of two new diblock copolymer systems, poly(butadiene-*b*-*tert*-butyl methacrylate) (BBMA) and poly(ethylene-*b*-*tert*-butyl methacrylate) (EBMA). The EBMA system was synthesized from the BBMA by hydrogenation of the polybutadiene block, thus creating two systems at practically the same volume fractions and identical degrees of polymerization, but with different segment interaction parameters and conformational asymmetries. Hydrogenation of the butadiene block resulted in an increased incompatibility and to an asymmetric phase diagram. In one of the EBMA copolymers with a PE volume fraction $f_{PE} = 0.42$, crystallization of the PE blocks was confined by the cylindrical mesophase in a *fluid* matrix. Upon PE crystallization, the hexagonal order was found to improve significantly following a matrix-assisted reorganization.

1. Introduction

The rich phase behavior of diblock copolymers has attracted considerable interest from theory and experiment in the past two decades.[1] In Leibler's mean-field theory (MFT),[2] two variables are thought to determine the phase state of diblock copolymers: the volume fraction, f, and the product of the interaction parameter, χ, with the degree of polymerization, N (χN). For a symmetric diblock copolymer the theory predicts a second-order phase transition from the disordered to the lamellar phase by lowering temperature at the critical point ($\chi N = 10.495$, $f = {}^1/_2$). For very asymmetric diblock copolymers the theory predicts a first-order phase transition from the disordered phase to spheres packed in a body-centered-cubic (bcc) lattice. In addition, the theory provides an expression for the disordered phase structure factor, $S(q)$, which was employed in the description of the scattering profiles from disordered copolymers.

Despite the success of the theory, there have been several cases where the predicted phase diagram was inadequate in explaining the rich experimental features. For example, several experiments have identified the disorder-to-order transition as a first-order transition even for symmetric block copolymers.[3−5] Furthermore, experimental phase diagrams are more complex and asymmetric, allowing, for example, for a direct transformation from the disordered to the lamellar phase even for nonsymmetric compositions. These results motivated Fredrickson and Helfand[6] to introduce fluctuation corrections to Leibler's MFT for weakly segregated copolymers. They extended Brazovskii's Hartree approximation to demonstrate that systems in the new universality class exhibit a fluctuation-induced first-order transition in the place of the continuous second-order transition predicted by the MFT. Furthermore, self-consistent-field theory calculations[7] suggested that conformational asymmetry plays a dominant role on the order-to-disorder and order-to-order phase boundaries. The main effect is to shift the phase boundaries toward compositions richer in the segments with the higher asymmetry. This asymmetry has been attributed to differences in monomer volume and backbone flexibilities of the two blocks.

The more extensively investigated diblock copolymer systems are the poly(isoprene-*b*-styrene) (PI−PS)[8] and the poly(ethylene oxide-*b*-isoprene) (PEO−PI).[9] In these systems four equilibrium phases were found in the melt: lamellar (lam), hexagonally packed cylinders (Hex), a bicontinuous structure with $Ia\bar{3}d$ space group symmetry (known as the Gyroid phase), and spheres packed in a bcc lattice. Other systems investigated to a smaller extent are the poly(ethylene-*b*-ethylene propylene) (PE−PEP),[10] poly(styrene-*b*-2-vinylpyridine) (PS−P2VP),[11] poly(ethylene propylene-*b*-ethylethylene) (PEP−PEE),[12] and poly(ethylene-*b*-ethylethylene) (PE−PEE).[13] There are some intriguing features with respect to the appearance and origin of the complex phases in these phase diagrams. All phase diagrams were found to be asymmetric around $f = {}^1/_2$ due to the conformational asymmetry. The Gyroid phase was found only in systems with low N, suggesting that this structure is stabilized by fluctuations. Furthermore, the experimental phase diagrams allowed for direct transitions from the hexagonal and lamellar phases to the disordered phase.

Of particular interest are systems with one crystallizable block since the copolymer microdomains can serve as templates to control crystallization. Herein we investigate the phase state of two new diblock copolymer systems, poly(butadiene-*b*-*tert*-butyl methacrylate) (BBMA) and poly(ethylene-*b*-*tert*-butyl methacrylate) (EBMA), with different block mobilities [T_g(polybutadiene) = 208 K, T_g(poly(*tert*-butyl methacrylate)) = 293 K] and different volume-filling properties. Furthermore,

[†] Foundation for Research and Technology-Hellas.
[‡] University of Ioannina and Biomedical Research Institute (BRI-FORTH).
[§] University of Athens.
[⊥] Max-Planck Institut für Polymerforschung.

10.1021/ma020540b CCC: $22.00
Published on Web 10/04/2002

since the EBMA copolymers are obtained by hydrogenation from the BBMA copolymers, it is possible to investigate the phase behavior at a fixed number of monomers and volume fraction as a function of the strength of the segment−segment interactions (χ). The phase behavior was investigated with differential scanning calorimetry, rheology, and small- and wide-angle X-ray scattering (SAXS/WAXS) techniques, utilizing 11 samples of varying molecular weight and block volume fractions.

2. Experimental Section

I. Synthesis. a. Synthesis of Poly(butadiene(high)1,4-*b*-*tert*-butyl methacrylate) Copolymers: The diblock copolymer precursors containing polybutadiene (PB) with mainly 1,4 microstructure (the 1,2 microstructure was 8%) and *tert*-butyl methacrylate blocks were synthesized by anionic polymerization with high-vacuum techniques.[14] Butadiene monomer was first polymerized, using *sec*-BuLi as the initiator and benzene as the solvent. The solution of living PBLi was then transferred into ampules equipped with break-seals. Each of these ampules was attached to a second polymerization reactor, washed with diphenylhexyllithium (DPHL), and rinsed with THF. To this reactor, ampules containing purified diphenylethylene (DPE) in hexane (in 2−5 times molar excess of the living ends), LiCl in THF (5 times molar excess over the living ends), and *tert*-butyl methacrylate (tBMA) monomer, purified over CaH_2 and trioctylalluminum just prior to use, were also attached. The reactor containing THF (the polymerization solvent, in 2.5 times volume excess over the volume of PBLi solution in benzene) was immersed into a dry ice/2-propanol bath at −78 °C, and DPE, LiCl, and PBLi were introduced by that order under stirring. tBMA was then distilled into the reactor, causing the deep red color of PBDPELi to disappear immediately. The polymerization was finally terminated with degassed methanol. The copolymers were precipitated in methanol and stabilized with 2,6-di-*tert*-butyl-*p*-cresol, after condensing the THF/benzene mixed solution in a rotor evaporator to about 30% of the initial volume. Addition of distilled water (10−20 vol %) into methanol was required for quantitative precipitation of the copolymers having a high poly(*tert*-butyl methacrylate) (PtBMA) content. The samples were thoroughly dried in a vacuum oven for a period of 1 week or more. The samples were denoted as BBMA followed by a number representing the order of sample synthesis.

b. Synthesis of Poly(ethylene-*b*-*tert*-butyl methacrylate) Copolymers. The block copolymers having a semicrystalline polyethylene (PE) block and an amorphous PtBMA block were synthesized by selective hydrogenation of the PB block using the Wilkinson catalyst system ($RhCl(PPh_3)_3$) in a Parr autoclave.[15] Toluene was the reaction solvent. Wilkinson catalyst was added in a 1:400 molar ratio of catalyst to double bonds. Triphenylphosphine (1:3 molar ratio of catalyst to free triphenylphosphine) was also used. The reaction was run under a 100 psi H_2 pressure and at a temperature of 373 K for 24−48 h. The final product was precipitated in methanol several times to remove the catalyst and was dried under vacuum. Samples were denoted as EBMA followed by the number of the corresponding precursor.

All block copolymer precursors were molecularly characterized by SEC, membrane osmometry, LALLS, and NMR to determine molecular weights, molecular weight polydispersity, and composition. The extent of hydrogenation reaction was checked by solid-state ^{13}C NMR and found to be quantitative. The molecular characteristics of all samples are given in Table 1.

II. Small-angle X-ray scattering (SAXS). An 18 kW rotating-anode X-ray source (Rigaku) was used with a pinhole collimation and a two-dimensional detector (Siemens) with 1024 × 1024 pixels. Measurements of 30 min long were made at intervals of 5 K on heating and subsequent cooling within the range 298−553 K, with stability better than ±0.2 K using an appropriate computer program.

Table 1. Molecular Characteristics of the Poly(butadiene-*b*-*tert*-butyl methacrylate) (BBMA) and of the Poly(ethylene-*b*-*tert*-butyl methacrylate) (EBMA) Diblock Copolymers

sample	$M_{w,\,total}$[a]	$M_{n,total}$[b]	$M_{n.PB}$[b]	M_w/M_n[c]	f_{PB}[d] (f_{PE})
BBMA 1 (EBMA 1)	16900	15500	11400	1.04	0.76 (0.77)
BBMA 7	6000	5000	3200	1.04	0.67
BBMA 2 (EBMA 2)	20000	18300	11400	1.04	0.65 (0.67)
BBMA 9 (EBMA 9)	7100	6300	3200	1.06	0.54 (0.55)
BBMA 6 (EBMA 6)	9200	8500	3200	1.07	0.41 (0.42)
BBMA 3 (EBMA 3)	33600	30800	11400	1.09	0.40 (0.41)

[a] By low-angle laser light scattering (LALLS) in toluene at 37 °C. [b] By membrane osmometry (MO) in toluene at 37 °C. [c] By size exclusion chromatography (SEC) in THF at 30 °C. [d] ^1H NMR in $CDCl_3$ at 30 °C.

Table 2. Transition Temperatures, Morphologies, and Physical Characteristics of the Poly(butadiene-*b*-*tert*-butyl methacrylate) (BBMA) Copolymers

sample	$T_{g,1}$ (K)	$T_{g,2}$ (K)	T_{ODT} (K)	ΔH_{ODT} (J/g)	morphology	f_{PB}
BBMA1	178	323	385	2	Hex $\xrightarrow{386\ K}$ Dis	0.76
BBMA7					Dis	0.67
BBMA2	178	343			Lam	0.65
BBMA9					Dis	0.54
BBMA6	183	335			Dis	0.41
BBMA3	176	367			Lam	0.40

III. Simultaneous SAXS/WAXS Synchrotron X-ray Measurements. Real time-resolved synchrotron small-angle and wide-angle X-ray scattering SAXS/WAXS measurements have been performed for one of the samples (EBMA6) at the X27C beamline of the National Synchrotron Light Source at Brookhaven National Laboratory. The wavelength of the X-rays was 0.1366 nm. Two position-sensitive detectors were used: one at small angle at a distance of 1.918 m from the sample and the other at a wide-angle setting of about 45° to the sample. The sample thickness was about 1 mm. The sample was set initially at an oven at 383 K for 10 min and subsequently brought to the final preset temperature in another oven using a temperature jump unit available at X27C. Temperature equilibration within the sample takes about 100 s. Simultaneous SAXS/WAXS spectra were taken at intervals of 60 s to the end of the crystallization process.

IV. Differential Scanning Calorimetry (DSC). Thermal measurements were performed with a (i) Metler Toledo Star differential scanning calorimeter system and (ii) a Polymer Laboratories DSC, both calibrated with sapphire for the baseline and indium and tin for the temperature and heat of fusion. Data were subsequently analyzed with the appropriate software. Measurements were made at a constant heating and cooling rate of 10 K/min. For both series of samples two glass transition temperatures were identified in the ordered state corresponding to the PB (PE) and PtBMA blocks. In the case of BBMA6, the two glass temperatures were shifted, indicating mixing of the two phases. The T_g values in the BBMA and EBMA diblock systems are summarized together with the morphologies and transition temperatures in Tables 2 and 3, respectively. In one of the samples (BBMA1) a small exothermic peak (∼2 J/g), associated with the free energy of mixing, was observed at the order-to-disorder transition temperature (T_{ODT} = 386 K), in agreement with theoretical considerations predicting:[16]

$$\Delta H \approx \frac{R T_{ODT} f (1 - f)(\chi N)_{ODT}}{M_n} \qquad (1)$$

where R is the gas constant, N is the total degree of polymerization, and M_n is the total number-averaged molecular weight.

Apart from the glass temperature, all EBMA copolymers exhibit an endothermic (exothermic) peak on heating (cooling)

Table 3. Amorphous and Crystral Block Characteristics in Poly(ethylene-*b*-*tert*-butyl methacrylate) (EBMA) Copolymers[a]

sample	T_g (K)	T_m (K)	T_{ODT} (K)	ΔH_f (J/g)	X_c	d (nm)[b]	morphology	f_{PE}
EBMA1	321	373		63.7	0.30	24.2	$L_c \xrightarrow{373\ K}$ Hex	0.77
EBMA2	318	371		49.8	0.27	27.7	$L_c \xrightarrow{371\ K}$ Lam	0.67
EBMA9		368	410	37	0.24	14.6	$L_c \xrightarrow{368\ K}$ Lam $\xrightarrow{413\ K}$ Dis	0.55
EBMA6	323	358		18	0.15	17.3	$Hex_c \xrightarrow{358\ K}$ Hex	0.42
EBMA3	305	371		25	0.22	34.1	$L_c \xrightarrow{371\ K}$ Hex	0.41

[a] $f_A = (m_A)/(m_A+m_B)(\rho_{PA}/\rho_{BM})$; A = poly(butadiene/ethylene) monomer; PA = poly(butadiene/ethylene), B = poly(*tert*-butyl methacrylate) monomer, BM = poly(*tert*-butyl methacrylate) m_A = (54/28) g/mol, m_B = 142 g/mol; amorphous densities (g/cm^3): ρ_{PB} = 0.895; ρ_{PE} = 0.855; ρ_{BM} = 1.02.[25] [b] Lamellar spacing (L_c) or intercylinder distance (Hex_c) in the crystalline phase: $d = 2\pi/q^*$ (L_c) or $d = 7.26/q^*$ (Hex_c); crystal density: $\rho_{PE,c}$ = 1.0 g/cm^3.

characteristic of the melting (crystallization) of the PE block. From the heat of fusion, ΔH_f, and the weight fraction of the individual PE blocks, w_{PE}, the degree of crystallinity, X_c, was calculated as

$$X_c = \frac{\Delta H_{f,PE}}{\Delta H^0_{f,PE} w_{PE}} \quad (2)$$

where $\Delta H^0_{f,PE}$ (= 277 J/g) is the heat of fusion of a crystalline polyethylene. The degree of crystallinity and the domain spacing for the EBMA series are summarized in Table 3. In the calculation of the domain spacing we have used $d = 2\pi/q^*$ for crystalline lamellar structures and $d = 7.26/q^*$ in the Hex_c case (intercylinder distance).

V. Rheology. An advanced rheometric expansion system (ARES) equipped with a force-rebalanced transducer was used in the oscillatory mode. Depending on the sample and T range two transducers were used with 2000, 2 g·cm and 200, 0.2 g·cm upper and lower sensitivity, respectively. The samples were prepared on the lower plate of the 25 mm diameter parallel plate geometry setup and were heated under a nitrogen atmosphere until they could flow. Subsequently, the upper plate was brought into contact, the gap thickness was adjusted to 1 mm, and the sample was slowly cooled to the desired starting temperature. The storage (G') and loss (G'') moduli were monitored in different types of experiments. First, the linear and nonlinear viscoelastic ranges were identified, by recording the strain amplitude dependence of the complex shear modulus $|G^*|$. In all subsequent experiments strain amplitudes within the linear viscoelastic range were used (typically below 2%). These experiments involved (i) isochronal temperature scans within the range 298−413 K (heating and cooling) aiming to identify the transition temperatures, (ii) isothermal frequency scans for temperatures in the range 303−413 K and for frequencies $10^{-2} < \omega < 10^2$ rad/s with a strain amplitude below 2%, and (iii) isochronal/isothermal kinetic experiments at ω = 1 rad/s for BBMA1.

VI. Optical Microscopy. A Zeiss Axioskop 2 polarizing optical microscope was used together with a Linkham heating stage (THMS 600) and a TP93 temperature programmer. The experiments were made by heating the EBMA6 copolymer to 373 K followed by fast cooling to temperatures where PE is able to crystallize. The system is capable of monitoring the kinetics in real time by continuous recording using a CCD camera ($^1/_2$ in. SONY color camera) and a fast frame grabber (capable of up to 50 frames/s).

3. Results and Discussion

I. The Poly(butadiene-*b*-*tert*-butyl methacrylate) System. Three of the BBMA copolymers are in the disordered state (BBMA6, BBMA7, and BBMA9), two are microphase-separated up to the highest measurement temperature (BBMA3 and BBMA2), and one (BBMA1) undergoes an order-to-disorder transition at an experimentally accessible temperature (T_{ODT}^{BBMA1} = 386 K). Typical SAXS spectra of some of the BBMA diblock copolymers are shown in Figure 1. The copolymers BBMA2 (f_{PB} = 0.65) and BBMA3 (f_{PB} = 0.4) form a lamellar structure whereas BBMA1 (f_{PB} = 0.76) forms hexagonally packed cylinders as indicated by the positions of the main and higher-order peaks (relative peak positions 1:√3:√7). The BBMA1 copolymer stayed in the hexagonal microphase up to 386 K and then disorders, as indicated from the disappearance of higher-order reflections in the SAXS spectra (not shown). The transition is accompanied by discontinuities in the primary peak intensity, peak position, and peak width at the order-to-disorder transition temperature which are depicted in Figure 2 as a function of inverse temperature. In the low-temperature region (up to 333 K), the primary peak position at q^* is hardly temperature-dependent, reminiscent of the glassy state of the material. At higher temperatures, q^* increases linearly with inverse temperature (associated with chain contraction) and is discontinuous at the T_{ODT}, as has been observed earlier with asymmetric P(I-*b*-S) diblock copolymers.

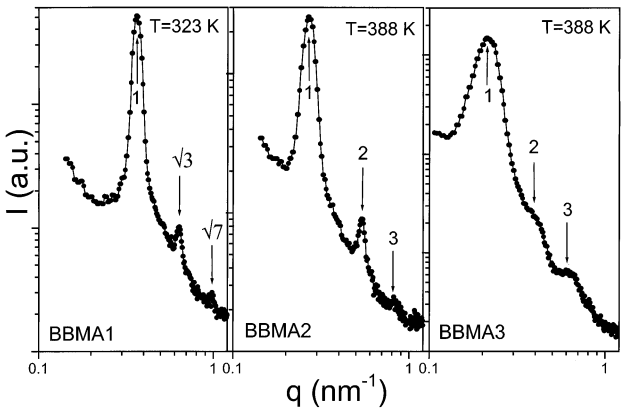

Figure 1. SAXS profiles of the BBMA copolymers with ordered mesophases. BBMA1: hexagonal packed cylinders (Hex) up to 386 K (relative peak positions 1:√3:√7). BBMA2: Lamellar (Lam) (relative peak positions 1:2:3). BBMA3: Lam (relative peak positions 1:2:3). BBMA2 and BBMA3 form a Lam phase over the entire temperature range investigated.

The accessible disordered phase in BBMA1 allows for the determination of the interaction parameter from the scattering profiles. In Figure 3 the SAXS profiles of

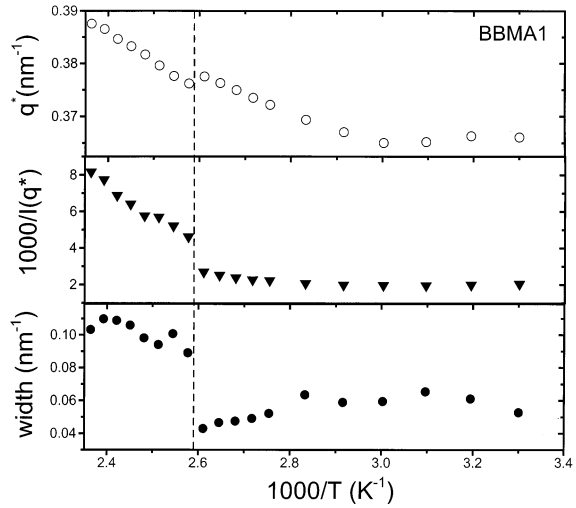

Figure 2. Temperature dependence of the primary SAXS peak reflection of BBMA1 showing discontinuities in peak position, intensity, and width at the order-to-disorder transition (T_{ODT} = 386 K).

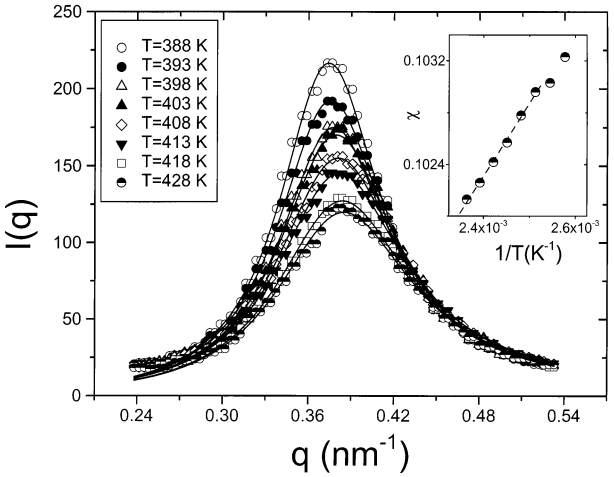

Figure 3. Small-angle scattering profiles from BBMA1 at temperatures above T_{ODT} (386 K) together with the results from the fits to Leibler's MFT (lines). In the inset, the obtained interaction parameter, χ, is plotted as a function of inverse temperature. The line is the result of a linear fit to the highest temperature data points resulting in the dependence: $\chi = 5.64/T + 0.089$.

BBMA1 are plotted against the scattering wave vector q, corresponding to temperatures near but above the order-to-disorder transition temperature. Leibler's MFT is used for the description of the disordered structure factor, $S(q)$, as[2]

$$\frac{1}{S(q)} = \frac{F(x,f)}{N} - 2\chi N \qquad (3)$$

where χ is the interaction parameter and $F(x,f)$ is a certain combination of Debye functions. There is a good agreement between theoretical predictions and experimental data in the disordered state. In the inset, the calculated values of the χ parameter are plotted as a function of inverse temperature. A linear fit to the higher temperature values gives rise to the following dependence:

$$\chi_{B-tBMA} = 0.089 + \frac{5.64}{T} \qquad (4)$$

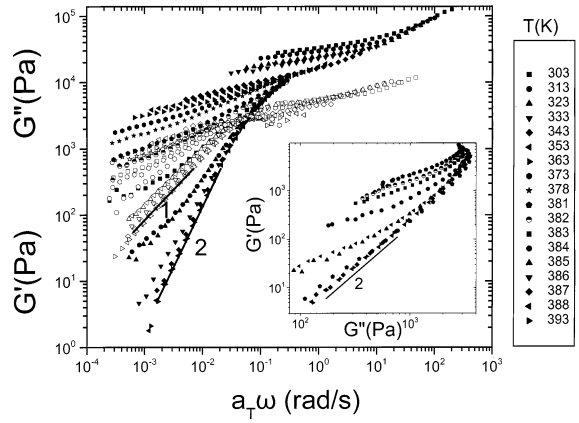

Figure 4. Frequency dependence of the storage (G', filled symbols) and loss (G'', open symbols) moduli of BBMA1 at different temperatures as indicated. Data are shifted with respect to frequency with a T-dependent shift factor a_T to the corresponding reference spectrum at 303 K. The Newtonian behavior ($G' \sim \omega^2$ and $G'' \sim \omega$) in the disordered phase (i.e., at T > 386 K) is replaced at lower temperatures by a rubbery-like state related to the unrelaxed microdomain morphology. In the inset the same data are plotted in the G' vs G'' representation and results in an identical transition temperature.

Notice that the MFT predicts that the transition should take place to a cubic phase instead of the hexagonal structure found here. When fluctuations are taken into account, transitions from a hexagonal mesophase to the disordered state are allowed. The $\chi(T)$ found in the BBMA system is comparable to that in the poly(ethylene-*b*-ethylene propylene) (PE−PEP) system examined earlier.[10] Moreover, the obtained morphologies for BBMA (Lam: $f_{PB} = \langle 0.40-0.65 \rangle$; Hex: $f_{PB} = 0.76$, Hex → Dis at $T \approx 386$ K) are also in agreement with the PE−PEP phase diagram.

It is well-known that the order-to-disorder transition has a strong influence on the viscoelastic properties of the composite material.[10,4] Because of the distinctly different viscoelastic contrast of the ordered and disordered states, low-frequency rheology is a very sensitive tool for detecting the dissolution of ordered microstructures. Isochronal measurements of the storage modulus performed at low frequencies with low strain amplitudes by slowly heating the copolymer provides a good way of locating the T_{ODT}. The former is an apparent transition temperature, and the way to extract the equilibrium order-to-disorder transition (T_{ODT}^0) has been described in the literature[17] in a way analogous to the equilibrium melting temperature in semicrystalline homopolymers. In Figure 4, we first discuss the result of the dynamic frequency sweeps in the vicinity of the T_{ODT}. Different sets of the storage and loss moduli data from different temperatures have been shifted along the frequency axis, using a single T-dependent shift factor, a_T, to the corresponding spectrum at the reference temperature (T_{ref} = 303 K). The "master curve" has been obtained by overlapping the high-frequency part of the spectra using the time−temperature superposition principle (tTs). At $T > T_{ODT}$, the tTs holds and the moduli exhibit typical terminal behavior ($G' \sim \omega^2$ and $G'' \sim \omega$). When examined over the whole temperature range, however, the tTs is violated due to the order-to-disorder transition which drives the system from the disordered state to a particular ordered morphology (hexagonally packed cylinders in this case). Thus, below the T_{ODT}, there is a breakdown of tTs at low frequencies, and the Newtonian

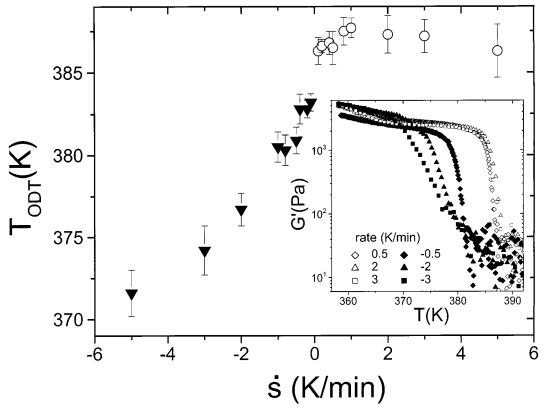

Figure 5. Dependence of the (apparent) order-to-disorder transition temperature of BBMA1 on the heating (circles) and cooling (inverse triangles) rates during the isochronal ($\omega = 1$ rad/s) temperature experiments. In the inset the storage modulus is shown for three different heating (open symbols) and cooling (filled symbols) rates. Notice that the transition temperature depends only slightly on the heating rate, whereas on cooling, the disordered phase can be effectively undercooled by as much as 20 K.

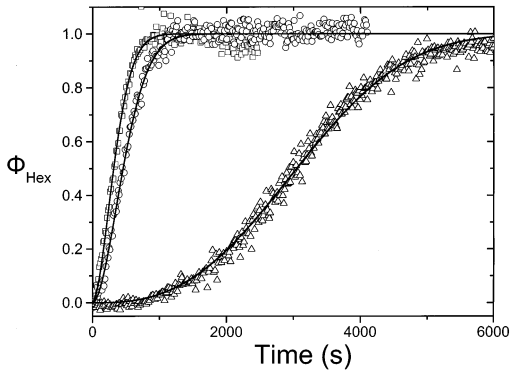

Figure 6. Evolution of the volume fraction of the Hex phase (φ_{Hex}) following T-jumps from 393 K corresponding to the disordered phase, to 379 (squares), 380 (circles), and 381 K (triangles) as calculated from the $G'(t)$ and $G''(t)$ dependencies. The lines are fits to the Avrami equation (see text).

behavior of the disordered state is replaced by a rubbery state related to the unrelaxed ordered morphology. On the basis of these arguments, we can assign the T_{ODT} at 386 K, in excellent agreement with the SAXS results.

Strictly speaking, the use of tTs is not permitted in systems with a T-dependent internal structure such as block copolymers, and an alternative method has been proposed to extract the transition temperature by plotting the logarithm of the storage moduli as a function of the logarithm of the loss moduli for the different temperatures (known as the Han representation[18]). In this representation the ODT corresponds to a temperature where the slope attains a value of 2. The result of this representation is shown in the inset to Figure 4 and reveals an identical transition temperature.

The transition temperature is affected by the heating/cooling rate during the isochronal experiment. The results of the rate-dependent isochronal measurements on the T_{ODT} are shown in Figure 5 as a function of the heating and cooling rates. There is a strong hysteresis, as expected for first-order transitions, which is more pronounced upon cooling than upon heating (structure making vs structure breaking). On slow cooling, the ordering temperature is the highest since the system orders under quasi-isothermal conditions. Notice that the apparent melting temperature on the subsequent heating experiment with the same (slow) rate is not the highest as one would expect from the generalized Gibbs−Thomson equation, predicting a grain size dependence on supercooling (an effect proportional to the surface-to-volume ratio of grains[17]). This can be explained by the interference of the nucleation process with growth phenomena during slow cooling. We assign the T_{ODT} as the transition corresponding to the slowest heating rate (0.1 K/min), and this is in agreement with the transition temperature obtained from Figure 4.

The large supercooling calls for pronounced kinetic effects. To explore the disordered-to-hexagonal lattice transformation, we performed kinetic experiments starting from an initial temperature of 393 K, corresponding to the disordered state, followed by quenching to different final temperatures at 379, 380, and 381 K, corresponding to the ordered state. The evolution of the storage and loss moduli was recorded under isothermal conditions. Both moduli showed a sigmoidal shape with distinct plateaus at short and long times representing the initial undercooled disordered and final ordered phases, respectively. At intermediate times the system is regarded as a composite material made of the two phases with a proportion which evolves with time. Such kinetics are typical for block copolymers and suggest a nucleation and growth mechanism.[4] To analyze the ordering kinetics in terms of a nucleation and growth mechanism, the time dependence of the volume fraction of the ordered phase is needed. To extract the volume fraction of the cylindrical phase from the $G'(t)$ and $G''(t)$ dependencies, we have used a simple mechanical model which assumes that the modulus is a linear combination of the moduli of the Hex and Dis phases as

$$G^* = \phi_{Hex} G^*_{Hex} + \phi_{Dis} G^*_{Dis} \qquad (5)$$

where ϕ_{Hex} and $\phi_{Dis} = 1 - \phi_{Hex}$ are the volume fractions of the Hex and Dis phases, respectively.

The evolution of the extracted volume fraction corresponding to the hexagonal phase is shown in Figure 6 for the three temperatures investigated. The $\varphi(t)$ shown conforms to the well-known Avrami equation:[19]

$$\phi(t) = 1 - \exp(-zt^n) \qquad (6)$$

where z and n are the rate constant and the Avrami exponent, respectively, suggesting a nucleation and growth mechanism. The values of the exponent ($n \sim 2$) may suggest growth of one-dimensional objects with cylindrical symmetry from heterogeneous nuclei.

Overall, the BBMA diblock copolymer system has a moderate to low incompatibility which is reflected in the low χ values. The weak $\chi(T)$ explains the absence of any order-to-order transformations within the investigated T range. Furthermore, the phase transformation from the disordered state proceeds via nucleation and growth as implied by the presence of an endothermic peak in DSC at the order-to-disorder transition and from the associated nucleation and growth kinetics.

II. The Poly(ethylene-*b*-*tert*-butyl methacrylate) System. Half of the material from the BBMA series was hydrogenated to result in a new copolymer system: poly(ethylene-*b*-*tert*-butyl methacrylate) (EBMA), i.e., a material with exactly the same number of monomer units and almost identical volume fractions (f_{PE} in EBMA are only slightly higher than f_{PB} in the BBMA copolymers, due to the different densities of the respec-

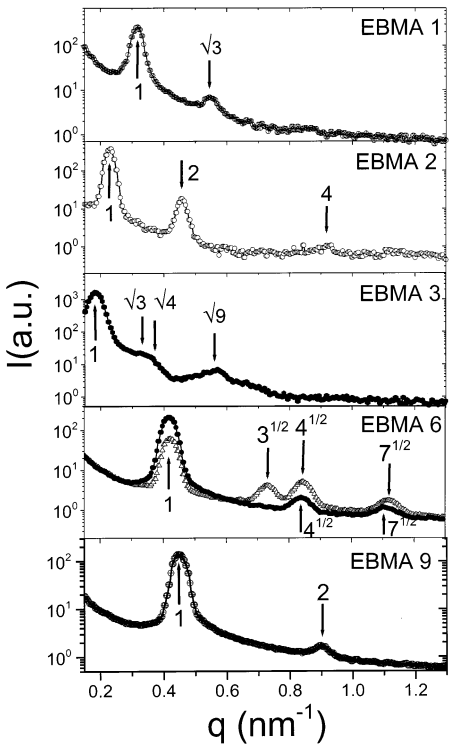

Figure 7. SAXS profiles of the EBMA series displaying ordered microstructures (all spectra correspond to 383 K except for the two spectra of EBMA6 shown at 353 and 333 K with open and filled symbols, respectively). EBMA1: hexagonally packed cylinders (Hex) (relative peak positions 1:√3). EBMA2: lamellar (Lam) (1:2:4). EBMA3: Hex (1:√3:√4:√7:√9). EBMA9: Lam (1:2). All copolymers of this series, with the exception of EBMA6, upon crystallization form a crystalline lamellar structure (L_c). EBMA 6 forms a Hex structure at $T > 358$ K (peaks with relative positions 1:√4:√7), but upon crystallization the Hex symmetry is preserved (peaks with relative positions 1:√3:√4:√7).

tive compounds), but with a drastically different interaction parameter χ_{E-tBMA}. Furthermore, the polyethylene block can crystallize, giving rise to at least one extra phase: the crystalline lamellar (L_c) phase (the branching content of PE is about 8%). The molecular and physical characteristics of this series are displayed in Tables 1 and 3, respectively. From the DSC measurements, besides the melting and glass transition temperature, the degree of crystallinity of the PE block was also obtained. Among the EBMA series, EBMA6 has the lower crystallinity (only 15%). The difference between the crystallization (T_c) and apparent melting temperatures (T_m') in a DSC circle was found to be 32 K in EBMA6 and about 20 K in the remaining EBMA copolymers, suggesting a possible different crystallization mechanism in the former.

In contrast to the BBMA series, where the lower molecular weight samples are disordered, all EBMA copolymers exhibit ordered morphologies up to very high temperatures, and only the diblock with the lowest molecular weight (EBMA9; $M_{n,total} = 6300$) disorders at an experimentally accessible temperature ($T_{ODT} = 413$ K). We point out that the corresponding diblock of the BBMA series, i.e., the BBMA9, was disordered at all temperatures investigated, implying an increase of the order-to-disorder transition by at least 100 K by hydrogenetion. This clearly shows that the χ value of the EBMA series is substantially higher from the BBMA series. Moreover, the observed order-to-order transformations in EBMA9 suggests also a stronger $\chi(T)$, but

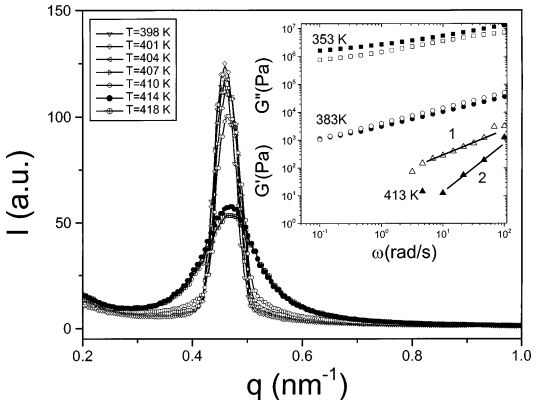

Figure 8. SAXS profiles of EBMA9, i.e., of the only copolymer of the EBMA series with an accessible disordered phase, at different temperatures as indicated, displaying an order-to-disorder transition at $410 < T < 414$ K. In the inset, the frequency dependence of the storage (filled symbols) and loss (open symbols) moduli of EBMA9 are shown at three temperatures ($T = 353$, 383, and 413 K). The combined results from SAXS and rheology suggest an order-to disorder transition temperature at 413 K.

the relatively high order-to-disorder transition temperature in that system precludes a more qualitative analysis for the $\chi_{E-tBMA}(T)$. On decreasing polyethylene content the following morphologies were obtained: $f_{PE} = 0.77$: Hex, $f_{PE} = \langle 0.66-0.55\rangle$: Lam, $f_{PE} = \langle 0.42-0.41\rangle$: again Hex, while in the BBMA series, the diblocks with corresponding volume fractions exhibited a lamellar morphology. Thus, the hexagonal phase in the EBMA system shifts to much higher volume fractions of the minority compound, PE, toward the right side of the phase diagram, as compared to the BBMA series. This asymmetry in the phase behavior is likely to result from the conformational asymmetry of the two polymers. For example, the high conformational asymmetry was responsible for the most asymmetric phase diagram in the poly(ethylene oxide-*b*-isoprene).[9] In the following we will discuss the phase state of each EBMA copolymer in more detail.

In Figure 7 the SAXS profiles of the five EBMA samples are shown as a function of q. For reasons of clarity, the scattering profiles in the L_c phase are not included but show broad peaks shifted to lower q values due to chain extension upon crystallization (except of EBMA6 to be discussed separately later). EBMA1 ($f_{PE} = 0.77$) and EBMA3 ($f_{PE} = 0.41$), form a crystalline lamellar structure upon crystallization, while in the melt the SAXS peaks at relative positions 1:√3 (EBMA1) and 1:√3:√4:√7:√9 (EBMA3) indicate the formation of a hexagonal mesophase which did not disorder up to the highest measured temperature. EBMA2 ($f_{PE} = 0.66$) and EBMA9 ($f_{PE} = 0.55$) have a lamellar structure in the melt (SAXS peaks at relative positions 1:2:4 (EBMA2) and 1:2 (EBMA9)), and as expected, this morphology was preserved upon crystallization.

The only sample in the EBMA series with an accessible disordered phase is the EBMA9 ($M_{w,total} = 7100$, $f_{PE} = 0.55$) and SAXS together with rheology have been employed to locate the exact transition temperature. In Figure 8, the scattering profiles of EBMA9 are shown at some temperatures in the range $373 < T < 418$ K together with the viscoelastic response at selected frequency sweeps shown at three temperatures. The SAXS profiles display a sudden drop in peak intensity

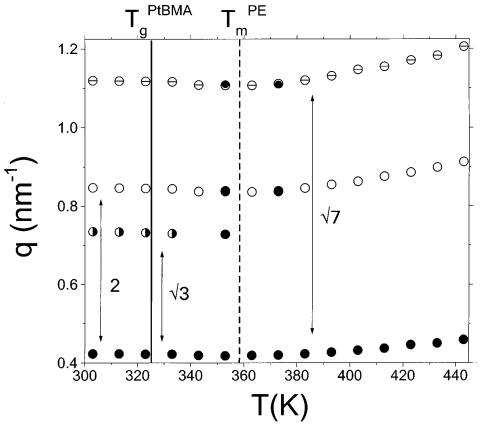

Figure 9. Temperature dependence of the SAXS primary reflection (filled symbols) and of the higher-order reflections (with relative positions 1:√3:√4:√7) of EBMA6 obtained on heating. Notice that the $\sqrt{3}q^*$ reflection disappears at the melting temperature of the PE block ($T_m^{PE} = 358$ K) shown with the vertical dashed line. Upon cooling, this reflection reappears at 333 K, that is, above the glass temperature of the PtBMA block, which is also indicated with the solid vertical line ($T_g^{PtBMA} = 323$ K).

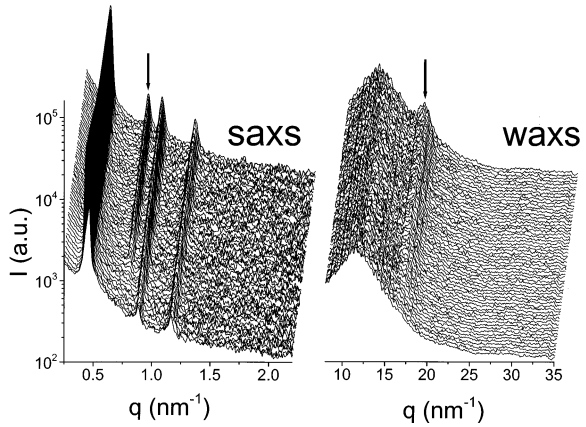

Figure 10. Simultaneous SAXS/WAXS synchrotron profiles of EBMA6 following a temperature jump from 383 to 333 K. Spectra are taken at intervals of 1 min. Arrows indicate the $\sqrt{3}q^*$ SAXS reflection and the (110) WAXS reflection corresponding to the most intense reflection of the PE orthorhombic unit cell.

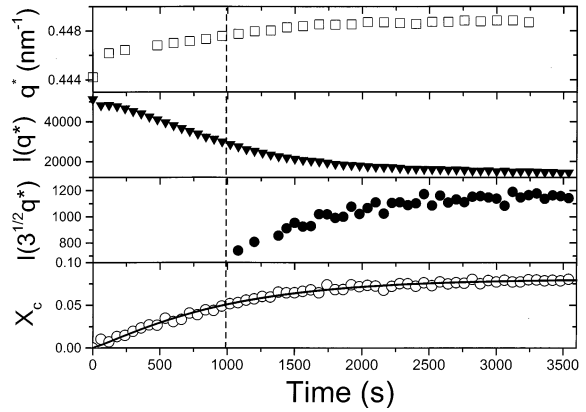

Figure 11. Evolution of the primary and secondary SAXS peak characteristics and of the crystallinity (X_c) obtained from WAXS following a temperature-jump from 383 to 333 K for EBMA6. The solid line is a fit to the Avrami equation. The vertical dashed line indicates the half-time of the crystallization process.

at temperatures in the range $410 < T < 414$ K. Over the same T range there are simultaneous discontinuities in the peak width and the main peak position (not shown here), suggesting an order-to-disorder transition. Thus, the combined SAXS and rheology measurements suggested a T_{ODT} at about 413 K for EBMA9.

III. Confined Crystallization in a Fluid Matrix. In the EBMA6 diblock copolymer ($f_{PE} = 0.42$, $M_n = 8500$, $X_c = 0.15$, $T_m = 358$ K) the SAXS results have shown that upon PE crystallization the melt mesophase is preserved. The two profiles shown in Figure 7, corresponding to 353 and 333 K (i.e., in the melt mesophase and below the PE crystallization), exhibit reflections at relative positions: 1:√4:√7 and 1:√3:√4:√7, respectively, indicating a Hex-to-Hex$_c$ transformation. PE crystallization takes place within the cylindrical mesophase in a fluid matrix, since the glass temperature of the PtBMA block forming the matrix is at 323 K, that is, about 10 K below the onset of crystallization. There are many examples where a block copolymer mesophase is destroyed upon crystallization[20−22] (a mechanism known as *break-out* crystallization) which takes place when the driving force for crystallization (a strong first-order transition) is so strong as to destabilize the melt morphology (usually when χ is not very high). There are also cases where the melt mesophase can be preserved upon crystallization of the minority phase (known as *confined* crystallization) when the matrix is glassy and acts as to "freeze" the melt mesophase despite the crystallization.[23] However, there are very few cases where the melt mesophase can act as a template for crystallization within a fluid matrix.[24] This last case requires very high block incompatibility (i.e., as in the EBMA series) and works for low degrees of crystallinity.

We followed the thermal stability of the Hex-to-Hex$_c$ transformation by performing several cooling and subsequent heating runs and found the transition to be thermally reversible. In Figure 9, the SAXS peak positions of EBMA6 are plotted as a function of temperature obtained by cooling from high temperature and subsequent heating. (For clarity, only some of the heating data points are plotted.) Notice that the $3^{1/2}q^*$ reflection appears above the PtBMA glass temperature (obtained from DSC). On heating, this reflection persists up to 358 K, i.e., the melting temperature of the PE crystals in the EBMA6 copolymer. Within the EBMA series, the EBMA6 is the only case where q^* remains unchanged upon crystallization (i.e., the epitaxial transformation), which again suggests that the melt mesophase is preserved.

To elucidate the mechanism of confined crystallization in EBMA6 (i.e., time scale, type of crystallization process), we investigated the crystallization kinetics using simultaneous SAXS/WAXS experiments at the X27C beamline at Brookhaven National Laboratory. The sample was heated to an initial temperature of 383 K, corresponding to the hexagonal melt mesophase, and brought to a final temperature of 333 K where the crystallization process was followed under isothermal conditions. Figure 10 shows the SAXS and corresponding WAXS spectra in 1 min intervals. The initial SAXS spectra exhibit reflections with relative positions at 1:√4:√7 whereas the corresponding WAXS spectra show a broad amorphous halo, suggesting an undercooled Hex melt mesophase. The final SAXS spectra show reflections with relative positions at 1:√3:√4:√7, and the corresponding WAXS spectra show a weak peak due to the (110) reflection of the PE orthorhombic unit

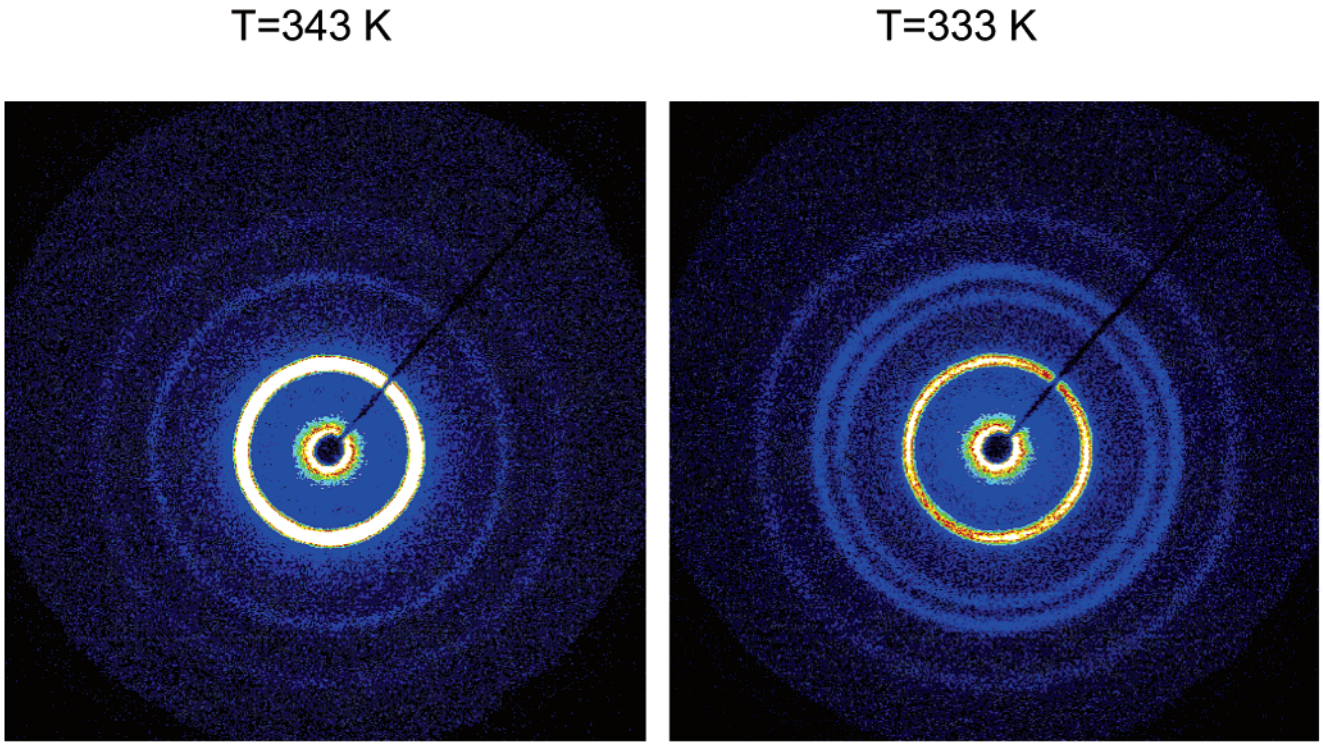

Figure 12. 2-D SAXS images obtained from an oriented EBMA6 fiber (the fiber orientation was nearly vertical) at two temperatures, 343 and 333 K, corresponding to the Hex and Hex_c mesophases, respectively.

cell. The low intensity of this reflection is in qualitative agreement with the DSC result. The intermediate SAXS/WAXS spectra reflect the growth of the $\sqrt{3}q^*$ SAXS and of the (110) WAXS reflections, suggesting that the appearance of the former is due to the PE crystallization. Notice the sharpness of this new reflection in the SAXS spectra, resulting in the unambiguous identification of the Hex_c structure.

The mechanism of PE crystallization can be understood by analyzing the SAXS/WAXS profiles. The evolution of the SAXS primary peak position at q^* and the intensity of the reflections at q^* and at $\sqrt{3}q^*$ are plotted in Figure 11, together with the degree of crystallinity obtained form the (110) WAXS reflection. We should mention here that the low crystallinity makes the peak deconvolution a difficult task and explains the lower crystallinity obtained in WAXS (about 9%) as compared to the corresponding value from DSC (about 15%). The Hex-to-Hex_c transformation proceeds epitaxially as indicated by the very small variation of q^* (below 1%). The drop of the primary peak intensity, $I(q^*)$, is due to the increased scattering in the PE domains upon crystallization which diminishes the contrast between the PtBMA and crystalline PE blocks. The $X_c(t)$ dependence conforms to the Avrami equation with a characteristic half-time, $t_{1/2}$, of 990 ± 13 s and an exponent of 1.13 ± 0.03. This low exponent may suggest that the whole crystallization process is determined by a (homogeneous) nucleation process alone since the nucleation density in the mesophases is much higher than in the homopolymer case. In addition, the sample was optically clear when examined with polarizing microscopy due to the nanoscale confinement that suppressed the formation of spherulites.

The appearance of the $\sqrt{3}q^*$ reflection in the SAXS spectra clearly relates to the process of PE crystallization. However, there are two possible ways of explaining the origin of this new reflection. First, it may represent

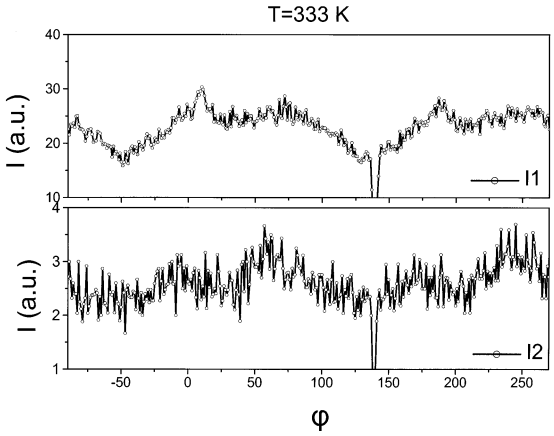

Figure 13. Azimuthally ring-averaged intensity of the arcs corresponding to the q^* and $\sqrt{3}q^*$ reflections from Figure 12 as a function of the azimuthal angle φ. Notice the similarity in the intensity variation for the two reflections, suggesting a common origin.

a new peak reflecting correlations among the PE crystals ($d \approx 7$ nm) within the PE cylinders (cylinder radius $R \approx 12$ nm). Second, it could reflect an improved order of the cylindrical microphase within the amorphous PtBMA matrix. To investigate further the two possibilities, we have prepared an EBMA6 fiber using a microextruder device (temperature 373 K, draw velocity 1 mm/min). SAXS were subsequently obtained on cooling from high T using a 2-D detector capable of revealing the anisotropy in orientation of the macroscopically oriented fiber. Two SAXS spectra obtained on cooling are depicted in Figure 12. The scattering pattern shown at 343 K reveals an intense ring corresponding to the main peak at q^* and higher-order rings with relative positions $1{:}\sqrt{4}{:}\sqrt{7}$ (Hex structure). At 333 K, the new reflection appears with relative position at $\sqrt{3}q^*$. The azimuthally integrated intensities of the two

peaks at q^* and $\sqrt{3}q^*$ are plotted separately in Figure 13 as a function of the azimuthal angle φ. Notice that the intensity variation in the latter (in the bottom of Figure 13) follows the intensity variation of the former (top of Figure 13), despite the scattering of the data points. This clearly excludes the possibility that the $\sqrt{3}q^*$ reflection is related to correlations among PE crystals, suggesting for its origin the improved hexagonal lattice order upon crystallization. The presence of a "fluid" matrix plays a significant role in assisting this reorganization.

4. Conclusion

The phase state of six poly(butadiene-*b*-*tert*-butyl methacrylate) and five poly(ethylene-*b*-*tert*-butyl methacrylate) diblock copolymers was investigated by differential scanning calorimetry, rheology, and small- and wide-angle X-ray scattering. The construction of a complete phase diagram requires normally about 20 or more diblock copolymers with appropriate compositions. The relatively small number of samples employed here precludes the construction of a complete phase diagram where all the equilibrium phases can be shown; however, the two systems allow for some important conclusions:

1. The interaction parameter in BBMA is relatively small and has a weak T dependence that explains the frequent occurrence of the disordered state for molecular weights below 10^4 and the absence of any order-to-order transformation. The disorder-to-order transition proceeds via nucleation and growth of anisotropic objects with the underlying symmetry of the final ordered phase.

2. Hydrogenation of the butadiene block results in a highly incompatible system at the same block length and composition with an inaccessible disordered state in most of the EBMA diblock copolymers investigated. Furthermore, the phase diagram shifts not only upward along the incompatibility axis (χN), due to $\chi_{E-tBMA} \gg \chi_{B-tBMA}$, but also along the composition axis due to the increased conformational asymmetry.

3. In one of the EBMA copolymers with $f_{PE} = 0.42$, crystallization of the PE blocks is *confined* by the cylindrical mesophase in a *fluid* matrix. Upon PE crystallization the hexagonal order improves significantly following a matrix-assisted reorganization.

Acknowledgment. The authors thank the scientific personnel of the X27C beam-line at BNL for beam-time and Dr. F.-J. Yeh for help during the synchrotron experiments. We acknowledge the support by a Marie-Curie fellowship (MCFI-1999-01036) to Dr. F. Schipper.

References and Notes

(1) Hamley, I. *The Physics of Block Copolymers*; Oxford University Press: Oxford, UK, 1998.
(2) Leibler, L. *Macromolecules* **1980**, *13*, 1602.
(3) Stühn, B. *J. Polym. Sci., Polym. Phys.* **1992**, *30*, 1013.
(4) Floudas, G.; Pakula, T.; Fischer, E. W.; Hadjicristidis, N.; Pispas, S. *Acta Polym.* **1994**, *45*, 176.
(5) Hashimoto, T.; Sakamoto, N.; Koga, T. *Phys. Rev. E* **1996**, *54*, 5832.
(6) Fredrickson, G. H.; Helfand, E. *J. Chem. Phys.* **1987**, *87*, 697.
(7) Matsen, M. W. *J. Phys. C: Condens. Matter* **2002**, *14*, R21.
(8) Khandpur, A. K.; Förster, S.; Bates, F. S.; Hamley, I. W.; Ryan, A. J.; Bras, W.; Almdal, K.; Mortensen, K. *Macromolecules* **1995**, *28*, 8796.
(9) Floudas, G.; Vazaiou, B.; Schipper, F.; Ulrich, R.; Wiesner, U.; Iatrou, H.; Hadjichristidis, N. *Macromolecules* **2001**, *34*, 2947.
(10) Rosedale, J. H.; Bates, F. S.; Almdal, K.; Mortensen, K.; Hajduk, D. A.; Gruner, S. M. *Macromolecules* **1995**, *28*, 1429.
(11) Schulz, M. F.; Khandpur, A. K.; Bates, F. S.; Almdal, K.; Mortensen, K.; Hajduk, D. A.; Gruner, S. M. *Macromolecules* **1996**, *29*, 2857.
(12) Bates, F.; Schulz, M. F.; Khandpur, A. K.; Förster, S.; Rosedale, J. H.; Almdal, K.; Mortensen, K. *Faraday Discuss.* **1994**, *98*, 7.
(13) Zhao, J.; Majumdar, B.; Schulz, M. F.; Bates, F. S.; Almdal, K.; Mortensen, K.; Hajduk, D. A.; Gruner, S. M. *Macromolecules* **1996**, *29*, 1204.
(14) Hadjichrisitidis, N.; Iatrou, H.; Pispas, S.; Pistikalis, M. *J. Polym. Sci., Polym. Chem.* **2000**, *38*, 3211.
(15) Balsamo, V.; von Gyldenfeldt, F.; Stadler, R. *Macromol. Chem. Phys.* **1996**, *197*, 3317.
(16) Hajduk, D. A.; Gruner, S. M.; Erramilli, S.; Register, R. A.; Fetters, L. J. *Macromolecules* **1996**, *29*, 1473.
(17) Floudas, G.; Pakula, T.; Velis, G.; Sioula, S.; Hadjichristidis, N. *J. Chem. Phys.* **1998**, *108*, 6498.
(18) Han, C. D.; Baek, D. M.; Kim, J. K.; Ogawa, T.; Sakamoto, N.; Hashimoto, T. *Macromolecules* **1995**, *28*, 5043.
(19) Avrami, M. J. *J. Chem. Phys.* **1939**, *7*, 1103; **1940**, *8*, 212; **1941**, *9*, 177.
(20) Rangarajan, P.; Register, R. A.; Adamson, D. H.; Fetters, L. J.; Bras, W.; Naylor, S.; Ryan, A. J. *Macromolecules* **1995**, *28*, 1422.
(21) Quiram, D. J.; Register, R. A.; Marchand, G. R. *Macromolecules* **1997**, *30*, 4551.
(22) Floudas, G.; Ulrich, R.; Wiesner, U.; Chu, B. *Europhys. Lett.* **2000**, *50*, 182.
(23) Loo, Y.-L.; Register, R. A.; Ryan A. J.; Dee, G. T. *Macromolecules* **2001**, *34*, 8968.
(24) Loo, Y.-L.; Register, R. A.; Ryan A. J. *Macromolecules* **2002**, *35*, 2365.
(25) Van Krevelen, D. W. In *Properties of Polymers*, 2nd ed.; Elsevier: Amsterdam, 1976.

MA020540B